https://doi.org/10.5194/esd-2019-26
Preprint. Discussion started: 3 June 2019

Earth System Dynamics
Discussions
Open Access
EGU

Contributions of climate change and groundwater extraction to soil moisture trends

Longhuan Wang[1,2], Zhenghui Xie[1*], Binghao Jia[1], Jinbo Xie[1], Yan Wang[1,2], Bin Liu[1,2], Ruichao Li[1,2], Si Chen[1,2]

[1]State Key Laboratory of Numerical Modeling for Atmospheric Sciences and Geophysical Fluid Dynamics, Institute of Atmospheric Physics, Chinese Academy of Sciences, Beijing 100029, China

[2]College of Earth Science, University of Chinese Academy of Sciences, Beijing 100049, China

Correspondence to: Zhenghui Xie (zxie@lasg.iap.ac.cn)

Abstract. Climate change affects water availability for soil, and groundwater extraction influences water redistribution by altering water demand, both of which significantly affect soil moisture. Quantifying their relative contribution to the changes in soil moisture will further our understanding of the mechanisms underlying the global water cycle. In this study, two groups of simulations were conducted with and without groundwater (GW) extraction (estimated based on local water supply and demand) from 1979–2010 using the land surface model CAS-LSM with four global meteorological forcing datasets (GSWP3, PRINCETON, CRU-NCEP, and WFDEI). To investigate the contribution of climate change and GW extraction, a trajectory-based method was used. Comparing the simulated results with the in-situ dataset of the International Soil Moisture Network (ISMN) and the satellite-based soil moisture product of the European Space Agency's Climate Change Initiative (ESA-CCI) indicated that the CAS-LSM reasonably reproduced the distribution of soil moisture, and well matched the temporal changes. Globally, our results suggested a significant decreasing trend in surface soil moisture (0.98 e−4 mm^3 mm^{-3} yr^{-1}) over the 32-year period tested. The drying trends were mainly observed in arid regions such as the tropical desert regions in North Africa and the Arabian Peninsula. While the wetting trends were primarily in tropical forested areas in South America and Northeast Asia. Climate change contributed 101.2% and 90.7% to global drying and wetting trends of surface soil moisture, respectively, while GW extraction accounted for −1.2% and 9.3%, respectively. In deep soil, GW extraction contributed 1.37% and −3.21% to the drying and wetting trends, respectively. The weak influence of GW extraction may be because this activity occurs in limited areas. GW extraction contributed more than 35% to the change in

https://doi.org/10.5194/esd-2019-26
Preprint. Discussion started: 3 June 2019

Earth System Dynamics
Discussions
Open Access
EGU

surface soil moisture in wetting areas where GW overexploitation occurs. GW is mainly extracted for irrigation to alleviate soil water stress in semiarid regions that receive limited precipitation, thereby slowing the drying trend and accelerating the wetting trend of surface soil. However, GW exploitation weakens the hydraulic connection between soil and aquifer, leading to deeper soils drying up. Overall, climate change dominated the soil moisture trends, but the effect of GW extraction cannot be ignored.

1. Introduction

Soil moisture plays a critical role in controlling the exchange of water, energy, and carbon between the land–vegetation–water–atmosphere system (Seneviratne et al., 2010; van den Hurk et al., 2011). Soil drying could increase the possibility of agricultural drought and fire (Dai et al., 2011), and affects plant transpiration, photosynthesis, microbial activity, and a number of biogeochemical processes. Significant decreasing trends in soil moisture can lead to water scarcity, threatening water supply and associated food production (Döll et al., 2009; Wisser et al., 2010; Albergel et al., 2012; Wada et al., 2013; Dai, 2013; Zhan et al., 2016). Soil moisture trends are affected by both climate (e.g., precipitation and temperature) and human activities (e.g., groundwater (GW) extraction). Climate change can affect water availability for soil (Dai, 2013; Wentz et al., 2007; Feng, 2016), and human activities influence the soil water content through altering the surface water flux of soil (Min et al., 2011; Douville et al., 2013; Feng, 2016). GW extraction, such as for irrigation, also has been shown to affect local soil moisture. However, it remains unclear which of these factors exerts more influence owing to the complex interactions involved. Therefore, quantifying the contribution of climate change and GW extraction to soil moisture trends will improve our understanding of how human activities affect soil water content and will help to determine the mechanisms underlying the global water cycle.

Traditionally, trends in soil moisture have been studied using ground-based observations (Robock et al., 2005), which provide a direct record of soil moisture and are used as reference measurements for calibrating other methods for measuring soil moisture (Yin et al., 2018). Since they are limited in space, require significant manpower for sampling (Seneviratne et al., 2010), and cannot always represent larger scales, remote sensing methods (e.g., passive and active microwave remote sensing) that provide global

https://doi.org/10.5194/esd-2019-26
Preprint. Discussion started: 3 June 2019

Earth System Dynamics Discussions
Open Access
EGU

55 coverage and excellent temporal sampling of soil moisture are widely used (Albergel et al., 2013).
56 Nevertheless, the accuracy of these measurements depends on the retrieval approach strongly, and
57 determining the contribution of climate and human activities is not easy. As a result, recent studies have
58 mostly relied on model estimates (Wei et al., 2008; Zhan et al., 2016).
59 Land surface models (LSMs) can represent trends in soil moisture at regional or global scales. Recently,
60 different LSMs have been developed to simulate soil moisture as a function of meteorological input
61 variables and soil and vegetation parameters (e.g., Kowalczyk et al., 2006; Lawrence et al., 2011; Best
62 et al., 2011). Much previous research has focused on the effect of climate change on soil moisture using
63 comprehensive LSMs forced with realistic forcing data (Berg et al., 2003; Guo et al., 2006; Wei et al.,
64 2008; Wang and Zeng, 2011). For the global average, precipitation had a dominant effect on the
65 variability of soil moisture at interannual to decadal time scales; however, temperature was the main
66 cause of the long-term trend in soil moisture. Increased soil drying in the transitional regions was
67 primarily caused by global warming, which is illustrated by regression analysis and LSMs (Cheng and
68 Huang, 2016). Since 1950, rising temperatures have contributed to 45% of the total soil moisture
69 reduction (Cai et al., 2009). In semiarid regions, precipitation and temperature are equally important to
70 the simulations of soil hydrological variables (Wang and Zeng, 2011). Jia et al. (2018) found that
71 precipitation controlled the direction of soil moisture changes using remote sensing data and modeling
72 of soil moisture in China. Recently, researchers have focused on incorporating human activity into the
73 hydrological processes of LSMs to assess the influence of anthropogenic activities on hydrological
74 variable simulations. For example, irrigation has been shown to affect soil water content through
75 increased local evapotranspiration and decreased temperatures near the surface (Yu et al., 2014; Zou et
76 al., 2014). GW over-extraction lowers GW tables, reduces total terrestrial water storage, weakens
77 hydraulic connections between aquifers and rivers, and may decrease lake area (Coe and Foley, 2001).
78 Wada et al. (2013) reported that human water consumption is one of the more important mechanisms
79 intensifying hydrological drought. GW exploitation caused drying in deep soil layers and wetting in
80 upper layers, lowering the water table and rapidly reducing terrestrial water storage with severe levels of
81 GW consumption (Zeng et al., 2016a, 2016b, 2017; Xie et al., 2018).
82 Most previous model-based studies have focused on the effects of climate conditions (precipitation and
83 temperature) on soil moisture characteristics. Thus, to our knowledge, the influence of anthropogenic
84 activities (GW extraction) on soil moisture has not been explicitly quantified. Therefore, the main

https://doi.org/10.5194/esd-2019-26
Preprint. Discussion started: 3 June 2019

purpose of our study was to assess the relative contribution of GW extraction and climate change to soil moisture trends. To address this issue, the historical land simulations of the Land Surface, Snow and Soil moisture Model Intercomparison Project (LS3MIP) were employed (van den Hurk et al., 2016). Four global meteorological forcing datasets covering the 20th century were used with the land surface model for the Chinese Academy of Sciences (CAS-LSM), which considers human water regulation (HWR) and the movement of frost and thaw fronts (Xie et al., 2018). We compared the simulations with in-situ observations and the ESA CCI satellite-based product to validate the capacity of the CAS-LSM to simulate soil moisture trends. Furthermore, we investigated the interannual variation and trends in simulated soil moisture. Finally, the response of soil moisture temporal variability to climate change and GW extraction was investigated, which can further our understanding of the relationship between soil moisture and climate.

Section 2 discribes the model used in this study, and describes the experimental designs, in-situ observations, and satellite-based data. Then Sect. 3 evaluates the soil moisture simulations in comparison with in-situ observations and satellite-based data. Also, the contributions of climate and GW extraction to soil moisture are discussed, while Sect. 4 outlines our conclusions.

2. Model, data, and experimental design

2.1 Description of CAS-LSM

Xie et al. (2018) incorporated GW lateral flow (GLF), Human Water Regulation (HWR), and the changes in the depth of frost and thaw fronts into CLM4.5 (Oleson, 2013) to develop the high-resolution CAS-LSM. For a detailed description of the physical processes within the CAS-LSM, see Xie et al. (2018). In the present study, only the HWR module was activated. Owing to the coarse resolution of the experiment, it is not possible to describe the water intake of the river, that is, the surface water. Therefore, only GW extraction was considered in our study. Here, only the processes associated with soil water are briefly described below.

The following equation represents the total water balance of the hydrological system:

$$\Delta W_{can} + \Delta W_{sfc} + \Delta W_{sno} + \Delta W_{soil} + \Delta W_a = \left(q_{rain} + q_{sno} + q_s + q_g - ET_{veg,ground,human} - q_{over} - q_{h2osfc} - q_{drai} - q_{rgwl} - q_{ice}\right)\Delta t \quad \text{Eq. (1)}$$

https://doi.org/10.5194/esd-2019-26
Preprint. Discussion started: 3 June 2019

Earth System Dynamics Discussions
Open Access
EGU

where the left side denotes the change in canopy water, surface water, snow water, soil water, and ice and water in the unconfined aquifer in turn. q_{rain} is rainfall, q_{sno} is snow, and q_s and q_g represent the rate of surface and GW water use respectively, some of which will return to the soil. q_{over} is surface runoff, q_{h2osfc} is runoff from surface water storage. q_{rgwl} and q_{ice} are liquid and solid runoff, respectively, from glaciers, wetlands, and lakes. q_{drai} is subsurface drainage and $ET_{veg,ground,human}$ is evapotranspiration from vegetation, ground, and human water use. Δt is the time step(s).

2.2 Experimental setup

In this study, GSWP3 (Kim et al., 2016), WFDEI (Haddeland et al., 2011; Weedon at al., 2014), CRU-NCEP (Viovy and Ciais, 2009), and PRINCETON (Sheffield et al., 2006) were used to run the offline model. The fields included were air temperature, wind speed, specific humidity, solar radiation, and precipitation. The GSWP3 is based on a dynamical downscaling of the 20th century reanalysis project (Compo et al., 2011), covering the entire 20th century and some of the 21st century (1901–2012) at 0.5° spatial resolution and 3-h intervals. The WATCH forcing data (WFD) are based on the ECMWF-ERA-40 reanalysis data, and were also at 0.5° resolution and 3-h intervals, ceasing in 2001. A subsequent project, EMBARCE, provided the WFDEI, which consisted of 3-h-interval ECMWF ERA-Interim reanalysis data interpolated to 0.5° spatial resolution (1979–2014). Thus, there are offsets for some variables in the overlap period with the WFD. The CRU-NCEP provided 6-h-interval data at 0.5° horizontal spatial resolution (1901–2010). The PRINCETON is based on 6-h-interval surface climate data from the NCEP-NCAR reanalysis. These data are available at 0.5° resolution and 3-h intervals. The version used in this study is from 1901–2012 with a real-time extension based on satellite precipitation and weather model analysis fields. General information about these datasets is summarized in Table 1. Four forcing datasets were bilinearly interpolated to construct a field to a uniform 0.9° × 1.25° to ensure that every simulation had the same soil and vegetation parameters.

We replaced the land cover data with the new generation of "land-use harmonization" (LUH2), which builds on past work from CMIP5 (Hurtt et al., 2011). In addition, monthly irrigation datasets (Zeng et al., 2016) were used for land model runs, which were developed based on the Food and Agriculture Organization of the United Nations (FAO) global water information system and the Global Map of Irrigation Areas, version 5.0 (GMIA5; Siebert et al., 2005) and reflected the actual levels of water consumption.

https://doi.org/10.5194/esd-2019-26
Preprint. Discussion started: 3 June 2019

Two sets of numerical experiments were conducted using the default CLM4.5 (hereafter referred to as CTL) and using the CAS-LSM with the HWR module activated (hereafter referred to as NEW). Thus, CTL and NEW contained four simulations, CTL-GSWP3, CTL-CRUNCEP, CTL-PRINCETON, and CTL-WFDEI (prefixed with NEW- for the NEW model). The CTL runs did not include GW extraction, while the NEW runs did include it. Therefore, the difference between the NEW and CTL models would provide a measure of the effect of GW extraction. Simulation spin up followed the TRENDY protocol (http://dgvm.ceh.ac.uk/node/9) by recycling the climate mean and variability from 20 years (1901–1920) of the meteorological forcing. Land use and CO_2 concentration were set to constant at the 1850 level during spin up. All simulations were conducted with horizontal spacing of 0.9° × 1.25°. However, there were differences among the four forcing datasets; therefore, the simulation period covers between 1901 and 2010 at a time step of 30 min. Considering that the ESA CCI was available from 1979–2010, our evaluation focused on the same time interval.

2.3 In-situ soil moisture and satellite-based data

To evaluate the capability of the CAS-LSM to simulate soil moisture variation, we retrieved in-situ soil moisture data from the International Soil Moisture Network (ISMN) (Robock et al., 2000; Dorigo et al., 2011; Dorigo et al., 2013). The ISMN is based on in-situ measurements from different regional monitoring projects. For our study, we used data from Africa, Asia, Europe, Australia, and North America networks. Stations with >75% of the observational data missing during the evaluation period were excluded. After which a subset of 225 stations remained (Fig. 3). There were only three dominant contiguous areas in the world (the central USA, the North China Plain, and northern India) with severe levels of GW extraction (Zeng et al., 2016b). Therefore, we focused on validating the ability of the model to accurately represent the soil moisture in these three areas. Further site information is presented in Table 2.

The European Space Agency's Climate Change Initiative (ESA CCI) involves remote sensing projects to monitor global key climate variables with feedback effects on climate change. Soil moisture was then included in 2010. There are three ESA CCI soil moisture products available based on the two types of sensors employed by the project: active microwave remote sensing, passive microwave remote sensing, and a combined product of both active and passive data. The active product was obtained using the SCAT scatterometer and the METOP-A satellite-equipped C-band scatterometer using the algorithm proposed

https://doi.org/10.5194/esd-2019-26
Preprint. Discussion started: 3 June 2019

by Wagner et al. (1999). The passive product includes observation data from four satellites, namely the tropical rainfall measuring mission microwave imager, the scanning multichannel microwave radiometer, the specific sensor microwave imager, and the advanced microwave scanning radiometer-Earth observing system. In the present study, we used the combined product (version 3.2), which covers 38 years from 1978–2016 at a daily temporal resolution.

2.4 Analysis method

Taylor's skill score (*S*) (Taylor, 2001) was used to quantitatively evaluate the spatial correlation of modeled soil moisture against the observations with standard deviations as follows:

$$S = \frac{4(1+R)^4}{(\sigma_f + 1/\sigma_f)^2(1+R_0)^4} \quad \text{Eq. (2)}$$

where σ_f is the ratio of the standard deviation of the simulations to the observations, R is the spatial correlation coefficient between the simulation and observation, and R_0 is the maximum possible spatial correlation coefficient. As the model variance approaches the observed variance (i.e., as $\sigma_f \to 1$) and as $R \to R_0$, the skill approaches 1. Thus, a higher value of S indicates a better model performance, and S = 1 when the simulation and observation data are identical.

All simulated datasets were converted to annual means by averaging for the growing season (March–October) before the trend analysis. Precipitation and temperature were treated the same as soil moisture. Trends were calculated using the nonparametric Mann-Kendall test and the Theil-Sen median slope (Sen, 1968) was used to delineate the trends.

To quantify the contribution of the climate and GW extraction to the trends in soil moisture, we used a trajectory method (Feng et al., 2014). Soil moisture in the CTL experiment represented the effect of climate on soil moisture trends and served as a reference for isolating the contribution of GW extraction. The contributions were calculated with area weight summarization as follows:

$$Con_{gw} = \frac{R_{gw}(T_{gw} - T_{ctl})}{T} \times 100\% \quad \text{Eq. (3)}$$

$$Con_{cm} = (1 - Con_{gw}) \times 100\% \quad \text{Eq. (4)}$$

where Con_{gw} and Con_{cm} are the global contributions of GW extraction and climate, respectively; R_{gw} is the area ratio of GW extraction in the drying or wetting areas; T_{gw} and T_{ctl} are the drying or wetting soil moisture trends in the GW and non-GW extraction regions, respectively; and T is the soil moisture trend in the global drying or wetting zones.

https://doi.org/10.5194/esd-2019-26
Preprint. Discussion started: 3 June 2019

Earth System Dynamics
Discussions
Open Access
EGU

198 Contributions of climate and GW extraction to certain grids were calculated as follows:

199 $$Con_{gw} = \frac{(T_{gw} - T_{ctl})}{T_{gw}} \times 100\% \quad \text{Eq. (5)}$$

200 $$Con_{cm} = (1 - Con_{gw}) \times 100\% \quad \text{Eq. (6)}$$

201 where Con_{gw} and Con_{cm} are the contributions of GW extraction and climate to each grid, respectively;
202 T_{gw} and T_{ctl} are the soil moisture trends in the NEW and CTL experiments, respectively.

203 **3. Results**

204 **3.1 Validation**

205 First, we compared the spatial distribution of simulated soil moisture with the ESA CCI product. Figure
206 1a, c, e, g shows the correlation coefficients between the ESA-CCI and the simulated top-10-cm soil
207 moisture from 1979-2010. The top-10-cm soil moisture is a weighted average of the first four soil layer
208 thicknesses (1.75, 2.76, 4.55, and 7.5 cm; the weights are 0.175, 0.276, 0.455, and 0.094, respectively).
209 The correlations between the simulated and ESA CCI data were significantly positive in most areas ($r >$
210 0.6). Modeled results were more accurate in humid and temperature zones especially in India and
211 Southeast Asia ($r > 0.9$). Results revealed that soil moisture dynamics cannot be well captured in northern
212 high-latitude areas (no correlation or negative correlations). This is partly due to the limited ability of
213 remote sensing technique in detecting soil moisture in frozen soils or under snow cover.
214 Figure 1b, d, f, h shows the differences between simulations and ESA CCI data. Soil moisture from all
215 forcing datasets presented similar broad patterns. ESA-CCI had lower soil moisture compared with the
216 simulated results from Europe and the eastern USA. While Fig. 1f shows the results from CRU-NCEP
217 are drier than those from the other three at high latitudes in the northern hemisphere. The simulation
218 results in WFD were wetter overall, and the PRINCETON drier in South America and Central Africa.
219 However, overall, the results from PRINCETON and GSWP3 simulation were closer. Soil moisture from
220 NEW was 0.06% to 0.09% higher than that from CTL. The area represented by NEW is irrigated; thus,
221 the top 10 cm of soil is wetter in NEW than in CTL. However, the increase in soil moisture was slight
222 (about 0.001 to 0.2 $mm^3\ mm^{-3}$). The differences between NEW and CTL indicate that there is a
223 significant increase in top-10-cm soil moisture in the central USA, the North China Plain, and North
224 India. The three areas with severe levels of GW extraction (Fig. 2).

https://doi.org/10.5194/esd-2019-26
Preprint. Discussion started: 3 June 2019


Earth System Dynamics
Discussions
Open Access
EGU

Figure 3 presents Taylor diagrams comparing the four NEW experiments with the in-situ ISMN observations over the eight subregions (see Table 2 for site details). Figure 3 clearly shows that the model can generally capture the changes in soil moisture in these regions. However, the performance of the model decreases as the soil depth increases. Results suggest that the standard deviation ratios at most stations in Africa, Australia, Europe, and North America were significantly close to 1, while those for India, Mongolia, China, and Former Soviet Union countries deviated from 1. Moreover, the different forcing datasets did not perform similarly. GSWP performed relatively poorly in deep soil in Europe, while PRINCETON provided a good estimation for Mongolia. CRUNCEP performed poorly in China and Mongolia. In general, GSWP and WFDEI performed well, except for Europe and Mongolia.

Three areas (the central USA, North China Plain, and northern India) with severe levels of GW exploitation were used as key areas for validation. The ground observations of soil moisture in the three regions were retrieved from the ISMN. The usable stations were as follows: seven sites on the North China Plain from 1981–1999, 15 sites in Colorado of central US from 2003–2010, and one site in Kanpur of northern India from 2011–2012. The regional soil moisture from observations and simulations were averaged from all stations and corresponding grid points. Before the comparison, hourly values from all stations were converted into a monthly time series. The soil layer depths in the CAS-LSM did not match those from the ground observations, and the depths of soil moisture observations varied among the three regions. Therefore, we used different methods for the different areas (Table 2).

We evaluated the performance of each forcing dataset over the three regions using Taylor's skill scores, as shown in Fig. 4 (left panel). As Fig. 4a shows, the individual forcing datasets show a varying ability to capture the soil moisture distribution. In the 0–10 cm soil layer, WFD performed well and had the highest skill scores (S = 0.86). Generally, all meteorological forcing datasets performed consistently well for the North China Plain in both the near-surface and deeper soil layers. Performance was also evaluated using a Taylor diagram as shown in Fig. 4d–f. GSWP captured the temporal variability of observed soil moisture with higher correlations than the other datasets. Correlations tended to cluster around 0.7, with the exception of CRUNCEP. Then, the correlations between observations and simulations decreased with soil depth. The radial distance from the origin represents the standard deviation of simulations relative to the standard deviation of observations. CRU-NCEP exhibited much higher ($\sigma_{sim}/\sigma_{obs}$ >1) variation than that of the in-situ observations.

https://doi.org/10.5194/esd-2019-26
Preprint. Discussion started: 3 June 2019

In the central US, WFD performed better with a higher skill score, and CRU-NCEP had the lowest score. Correlations between the simulated 5-cm soil moisture and observations (Fig. 4e) were all lower than 0.5. This may be because the offline runs do not consider the strong interaction between land and atmosphere. All simulations resulted in lower standard deviations than those for observations at 50 cm soil depth. This indicates that the true variability in soil moisture cannot be well reconstructed in this layer using the four forcing datasets tested herein. Errors were also associated with the varying degrees of mismatch between the soil layers of the observations and the model.

Owing to the limitations of the observational data in Kanpur, only three sets of data were compared in that area. Based on the skill scores, WFD and PRINCETON performed well at both 10 cm and 25 cm soil depths, and WFD performed better in deeper soil. The results of a correlation analysis indicated that the simulations from three meteorological forcing datasets (GSWP3, PRINCETON, and WFD) were able to capture the variation in soil moisture (Fig. 4f). Notably, the correlation was higher when considering the GW extraction, which was not obvious in the other two areas (Fig. 4f). This is because, according to FAO statistics, about 91% of GW extraction was to supply irrigation in India, whereas 64% and 38% of GW extraction was used by agriculture in China and the USA, respectively (Zeng et al., 2016b). Figure 4f shows that the relative standard deviations decreased as soil depth increased, which indicates relatively large errors of fluctuation in the deeper soil layers. Overall, WFDEI provided a better simulation with a higher correlation and a relative standard deviation close to 1.

3.2 Trends in soil moisture

Owing to the uncertainty in meteorological forcing, especially regarding precipitation, which had large differences between different forcing datasets (Table 3), the ensemble average approach was used here. Figure 5 presents the trends in surface soil moisture (0–10 cm), deep soil moisture (200–300 cm), precipitation, temperature, and GW extraction from 1979–2010 from the NEW experiment. Globally, results suggested a significant decreasing trend in surface and deep-soil moisture (−0.98 e−4 and −0.24 e−4 $mm^3\ mm^{-3}\ yr^{-1}$, respectively; $p < 0.05$) over the 32-year period, but the soil moisture trend from PRINCETON was not significant (Table 3). There was a consistent significant warming trend (about 0.016°C yr^{-1}; $p < 0.05$) and a non-significant decreasing precipitation trend ($p > 0.05$). Furthermore, the drying of the surface soil moisture slowed when considering the HWR. The global surface soil moisture decreased at a rate of −0.99 e−4 $mm^3\ mm^{-3}\ yr^{-1}$ without GW extraction. Conversely, the deep soil dried

https://doi.org/10.5194/esd-2019-26
Preprint. Discussion started: 3 June 2019

Earth System Dynamics
Discussions
Open Access
EGU

283 (−0.21 e−4 mm^3 mm^{-3} yr^{-1} in CTL) owing to the rapid lowering of the water table following GW
284 extraction, and the hydraulic connection between the soil and aquifer weakened. More specifically, GW
285 extraction slowed the drying of surface soils in drying areas and increased the wetting trend in wetting
286 areas. The trend in 1.3% of GW extraction areas changed from drying to wetting, with an average GW
287 extraction rate of 171 mm yr^{-1}. The opposite effect was observed in the deeper soil layers.
288 Figure 6 shows the spatial distribution of soil moisture trends from 1979–2010 obtained from simulations
289 of surface- and deep-soil moisture and ESA CCI. As the depth of the soil increased, the proportion of
290 apparent dryness increased. For the surface soil, the drying trends were mainly found in North Africa,
291 Central Asia, Southwestern USA, Southeast Australia. The wetting trends were primarily in northern
292 South America, northwest Africa, and northeast Asia. This result is consistent with those of previous
293 studies on satellite-based data (Feng, 2015; Dorigo et al., 2012). The trend in the deep soil was consistent
294 with that in the surface layer in most areas, except for Central Asia. Regions with a drying trend always
295 coincided with statistically significant increasing temperature. Many of the strong drying trends occurred
296 over regions that already have relatively low soil moisture. Drying trends were the most prominent in the
297 Sahel in northern Africa. This could be explained by deficits in precipitation during the 1970s and 1980s
298 (Hulme, 1992; L' Hôte et al., 2002). The majority of north Asia exhibited wetting trends with non-
299 significant increasing temperature. Wetting trends were found in the central US, India, and North China
300 Plain, but there were no significant changes.
301 We further evaluated the ratios of drying/wetting trends for surface and deep soil in different climate
302 regions using the Köppen-Geiger climate classification (Kottek et al., 2006). A brief description of the
303 climate classification is as follows: the first letter refers to the climate types: tropical (A), arid (B),
304 temperate (C), and cold (D). The second letter indicates the precipitation conditions: rainforest (f),
305 monsoon (m), and savannah (s) in tropical and desert (W) and steppe (S) in arid, dry summer (s), dry
306 winter (w), and without dry season (f) in temperate and cold climates. The third letter refers to hot (h)
307 and cold (k) in arid and hot summer (a), warm summer (b), cold summer (c), and very cold summer (d)
308 in temperate and cold climates. At the same time, we used the climate regions defined by Feng et al.
309 (2015), the first climate letter labelled Arid was the arid regions, the second letter "f" was the humid
310 regions and the other regions were the transitional regions. As Figure 7a shows, some arid regions became
311 significantly drier (16.9%) or wetter (9.8%); as did some humid regions (9.8% drier, 9.5% wetter) and
312 transitional regions (12.8% drier, 5.4% wetter). The area of increasing wetness in the Af subregion, which

https://doi.org/10.5194/esd-2019-26
Preprint. Discussion started: 3 June 2019

313 is characterized by tropical rainforests, comprised 22% of its total area. The Dfd subregion is
314 characterized by areas without a dry season and 42.6% of this region rapidly became wetter (about 1.2
315 e−3 mm^3 mm^{-3} yr^{-1}). Conversely, 21.5% of the BWh subregion, which is characterized by hot deserts,
316 was drying. In the Ds and Dw subregions, which have a hot summer or winter in a year, 30–40% was
317 drying out with a moisture decreasing rate more than −1.2 e−3 mm^3 mm^{-3} yr^{-1}. These results indicate
318 that the drying trends were mainly in arid regions, while the wetting trends were primarily in humid
319 regions. Figure 7b shows that there are proportionally more significant changes in the deeper soil layers.
320 However, the changes are not as great as those in the surface soil. In arid regions (BW and BS subregions),
321 the proportion of apparent drying exceeded 40%. In humid regions (Cfc, Dfc, and Dfd subregions), 30–
322 71% of these areas were significantly wetting. The climatic zone differences in deep soil changes were
323 basically consistent with those in the topsoil, except in Dwc and Dwd regions.

324 **3.3 Contribution of climate change and human activity to soil moisture trends**

325 The trend in soil moisture was basically consistent with climate change, but the role of GW extraction
326 was negligible. Then we quantified the relative contribution of climate and GW intake to the soil moisture
327 trends using the trajectory approach [Eqs. (*2*)–(*3*)]. Results showed that −1.2% of the significant drying
328 trends in the surface soil originated from GW extraction. Thus, the contribution of climate was 101.2%.
329 Regarding the wetting trends, the contribution was 9.3% for GW extraction, with climate contributing
330 90.7%. In deep soil, GW extraction contributed 1.37% and −3.21% to the drying and wetting trends,
331 respectively. This indicates that GW extraction only weakly contributes to global wetting and drying
332 trends. This is mainly due to the limited regions of GW extraction. The contribution of GW extraction to
333 surface soil moisture trends is presented in Fig. 8a. In the drying regions, GW extraction and climate
334 change accounted for −19.91% and 119.91%, respectively. In the wetting regions, the contributions were
335 11.55% and 88.45%, respectively. GW exploitation is mainly used for irrigation to increase moisture in
336 the surface soil, which slows the drying of the surface soil, promoting wetting. Figure 8b shows the
337 contribution of GW extraction in the deeper soil layers. GW extraction positively contributed to the
338 drying trends (109.7%) and negatively contributed to the wetting trends (−5.48%). This indirectly reflects
339 that GW exploitation weakens the hydraulic connection between soil and aquifers. In summary, GW is
340 exploited to provide irrigation, which alleviates water stress in the surface soil, and the deep soil dries
341 due to the loss of hydraulic connection.

https://doi.org/10.5194/esd-2019-26
Preprint. Discussion started: 3 June 2019

As shown in Fig. 8, the contribution of GW extraction mainly occurs in northern Africa, the North China Plain, and central US. Thus, the three regions were selected for further evaluation. Figure 9 further shows the relative contributions to soil moisture trends in three subregions. Contributions of GW extraction to surface soil moisture wetting and drying trends were evident on the North China Plain (drying, up to −62.39%; wetting, 77.74%), northern India (drying, up to −13.56%; wetting, 72.1%), and central US (drying, −57.42%; wetting, 38.51%). For deep soil, the contribution of GW extraction was: North China Plain (drying, 15.12%; wetting, −18.16%), northern India (drying, 56.54%; wetting, 2.07%), and central USA (drying, 23.8%; wetting, −20%). GW extraction can increase the water content of the surface soil, and thus leads to increased moisture in both humid and arid regions. The results revealed that GW extraction contributes more to the soil moisture trends in typical exploitation areas than in the regions without GW extraction. Climate change dominated the soil moisture trends, while the contribution of GW extraction at the regional scale was much greater than that at the global scale, especially in the areas with GW overexploitation.

4. Conclusions and discussion

In the present study, we quantified the relative contribution of climate and GW extraction to soil moisture trends using a LSM (CAS-LSM) that considers HWR based on four global meteorological forcing datasets. Comparing the simulations, the in-situ observational datasets, and the satellite-based ESA-CCI surface products demonstrated that the CAS-LSM is able to reliably represent soil moisture trends.

The main conclusions of this study are as follows. First, all four forcing data resulted in similar patterns of surface soil moisture, and have higher soil moisture than ESA-CCI. Results at the regional scale (Fig. 4) indicated that the uncertainty of the forcing data affected the simulated soil moisture. Therefore, the ensemble average results were used to reduce the uncertainty caused by the forcing data. Second, our results show a significant decreasing trend in surface and deep soil moisture over the 32-year period investigated. For the surface soil, GW extraction slowed the drying trend in drying areas and increased the wetting trend in wetting areas. This is because GW extraction is mainly used for irrigation as effective water input into the topsoil. While has opposite effect on deep soil when the hydrological connection between the aquifer and deep soil was weakened due to the extraction severely. Third, climate contributed 101.2% and 90.7% to global drying and wetting trends of surface soil moisture, while GW extraction had

https://doi.org/10.5194/esd-2019-26
Preprint. Discussion started: 3 June 2019

a relative weak effect on soil moisture (−1.2% and 9.3% for global drying and wetting, respectively). For deep soil, GW extraction contributed 1.37% and −3.21% to the drying and wetting trends. This is because there are limited areas that exploit GW. Regionally, GW extraction contributed more in regions with high water demand for irrigation, production, and human consumption. In typical water-use areas, including the North China Plain, Central US, and North India, GW extraction contributed more to the soil moisture trends than in the regions almost without GW extraction. In summary, climate change dominates the soil moisture trends, while GW extraction accelerates or decelerates soil moisture trends under climate change.

Our study demonstrated the effect of GW extraction on soil moisture. Future research should focus on developing strategies to adapt to climate change. At the same time, the effect of GW exploitation on regional soil moisture cannot be ignored. Over-exploitation weakens the hydraulic connection between soil and aquifer, which may affect root growth and development. Therefore, the development and utilization of water resources must consider the local ecological environment.

The mismatch of soil layers between the simulations and observations may affect the evaluation results. Also, our results indicate that it is necessary to consider human activities in LSMs, and improved descriptions of hydrological processes in LSMs are required. For example, GW extraction is assumed to be occur in the area it is consumed in. Moreover, meteorological forcing data can introduce uncertainty for simulation results. The precipitation data used in our study showed significant differences. The WFD precipitation evidently decreased (1.96 mm yr^{-1}), and the GSWP precipitation slightly decreased (0.16 mm yr^{-1}), while for CRU-NCEP and PRINCETON, precipitation slightly increased. Temperature varied similarly for all four forcing datasets (slightly increasing). The ensemble averaging method used in this study is not the optimum choice. However, considering that the purpose of this study was to explore the contribution of GW extraction to soil moisture trends, this simple averaging approach was reasonable. It is necessary to use a more appropriate averaging method to minimize the uncertainty caused by the forcing data in future work.

Future studies should focus on two aspects. First, GW extraction should be improved to reflect realistic levels of water consumption. Thus, simulations using the improved model would more accurately reflect hydrological effects and enhance water resource management. Second, since only the effect of HWR was discussed in this study, other human activities could also be considered. For instance, the association

https://doi.org/10.5194/esd-2019-26
Preprint. Discussion started: 3 June 2019

between soil moisture and land-cover change can be evaluated. Changes in land-surface cover affect the hydrothermal properties of the surface soil, which further affects soil moisture.

Acknowledgements. This work was jointly supported by the National Natural Science Foundation of China (Grants 41830967), the National Key R&D Program of China (2018YFC1506602) and by the Key Research Program of Frontier Sciences, CAS (QYZDY-SSW-DQC012). The ESA CCI soil moisture dataset was downloaded from http://www.esa-soilmoisture-cci.org; the in-situ soil moisture observations were downloaded from http://www.geo.tuwien.ac.at/insitu/data_viewer/ISMN.php.

References

Albergel, C., Rüdiger, C., Pellarin, T., Calvet, J. C., Fritz, N., Froissard, F., Suquia, D., Petitpa, A., Piguet, B., and Martin, E.: From near-surface to root-zone soil moisture using an exponential filter: An assessment of the method based on in-situ observations and model simulations. Hydrology and Earth System Sciences, 12(6), 1323–1337, 2008.

Albergel, C., de Rosnay, P., Gruhier, C., Muñoz-Sabater, J., Hasenauer, S., Isaksen, L., Kerr, Y., and Wagner, W.: Evaluation of remotely sensed and modelled soil moisture products using global ground-based in-situ observations, Remote Sens. Environ, 118, 215–226, 2012.

Albergel, C., Dorigo, W., Balsamo, G., Muñoz-Sabater, J., De Rosnay, P., and Isaksen, L., Brocca, L., de Jeu, R., and Wagner, W.: Monitoring multi-decadal satellite earth observation of soil moisture products through land surface reanalyses, Remote Sens. Environ, 138, 77-89, 2013.

Berg, Aaron A.: Impact of bias correction to reanalysis products on simulations of North American soil moisture and hydrological fluxes, Journal of Geophysical Research, 108(D16):ACL 2-1-ACL 2-15, 2003.

Best, M. J., Pryor, M., Clark, D. B., Rooney, G. G., Essery, R. L. H., Ménard, C. B., Edwards, J. M., Hendry, M. A., Porson, A., Gedney, N., Mercado, L. M., Sitch, S., Blyth, E., Boucher, O., Cox, P.

https://doi.org/10.5194/esd-2019-26
Preprint. Discussion started: 3 June 2019

422 M., Grimmond, C. S. B., and Harding, R.J.: The Joint UK Land Environment Simulator (JULES),
423 model description– Part 1: energy and water fluxes, Geosci. Model Dev, 4, 677–699, 2011.
424 Cai, W., Cowan, T., Briggs, P., and Raupach, M.: Rising temperature depletes soil moisture and
425 exacerbates severe drought conditions across southeast Australia, Geophysical Research Letters,
426 36(21), 272-277, 2009.
427 Calvet, J. C., Fritz, N., Froissard, F., Suquia, D., Petitpa, A., and Piguet, B.: In-situ soil moisture
428 observations for the CAL/VAL of SMOS: The SMOSMANIA network, Proceedings of the IEEE
429 International Geoscience and Remote Sensing Symposium (IGARSS), 2008.
430 Cappelaere, B., Descroix, L., Lebel, T., Boulain, N., Ramier, D., Laurent, J.-P., Favreau, G., Boubkraoui,
431 S., Boucher, M., Moussa, I. B., Chaffard, V., Hiernaux, P., Issoufou, H. B. A., Le Breton, E.,
432 Mamadou, I., Nazoumou, Y., Oï, M., Ottlé, C. and Quantin, G.: The AMMA-CATCH experiment
433 in the cultivated Sahelian area of south-west Niger - Investigating water cycle response to a
434 fluctuating climate and changing environment, Journal of Hydrology, 375(1-2), 34–51, 2009.
435 Cheng, S. J., and Huang, J. P.: Enhanced soil moisture drying in transitional regions under a warming
436 climate, Journal of Geophysical Research: Atmospheres, 121(6):2542-2555, 2016.
437 Coe, M. T., and Foley, J. A.: Human and natural impacts on the water resources of the lake chad basin,
438 Journal of Geophysical Research: Atmospheres, 106(D4), 3349-3356, 2001.
439 Compo, G. P., Whitaker, J. S., Sardeshmukh, P. D., Matsui, N., Allan, R. J., Yin, X., Gleason, B. E.,
440 Vose, R. S., Rutledge, G., Bessemoulin, P., Brönnimann, S., Brunet, M., Crouthamel, R. I., Grant,
441 A. N., Groisman, P. Y., Jones, P. D., Kruk, M. C., Kruger, A. C., Marshall, G. J., Maugeri, M.,
442 Mok, H. Y., Nordli, Ø., Ross, T. F., Trigo, R. M., Wang, X. L., Woodruff, S. D., and Worley, S.
443 J.: The Twentieth Century Reanalysis Project, Quart. J. Roy. Meteor. Soc., 137, 1–28, 2011.

https://doi.org/10.5194/esd-2019-26
Preprint. Discussion started: 3 June 2019

444 Dai, A. G.: Characteristics and trends in various forms of the palmer drought severity index during
445 1900–2008, Journal of Geophysical Research: Atmospheres, 116(D12), 2011.
446 Dai, A. G.: Increasing drought under global warming in observations and models, Nature Climate
447 Change, 3(1), 52-58, 2013.
448 de Rosnay, P. D., Gruhier, C., Timouk, F., Baup, F., Mougin, E., and Hiernaux, P., Kergoat, L., and
449 LeDantec, V.: Multi-scale soil moisture measurements at the Gourma meso-scale site in mali.
450 Journal of Hydrology (Amsterdam), 375(1-2), 241-252, 2009.
451 Dorigo, W.A., Wagner, W., Hohensinn, R., Hahn, S., Paulik, C., Xaver, A., Gruber, A., Drusch, M.,
452 Mecklenburg, S., van Oevelen, P., Robock, A., and Jackson, T.: The International Soil Moisture
453 Network: A data hosting facility for global in-situ soil moisture measurements, Hydrology and
454 Earth System Sciences, 15 (5), 1675-1698, 2011.
455 Dorigo, W.A., Jeu, R.D., Chung, D., Parinussa, R., Liu, Y., Wagner, W., and Fernández-Prieto, D.:
456 Evaluating global trends (1988–2010) in harmonized multi-satellite surface soil moisture,
457 Geophysical Research Letters, 39(18), 18405, 2012.
458 Dorigo, W. A. , Xaver, A. , Vreugdenhil, M. , Gruber, A. , Hegyiová, A., Sanchis-Dufau, A. D., Zamojski,
459 D., Cordes, C., Wagner, W., and Drush, M.: Global automated quality control of in-situ soil
460 moisture data from the international soil moisture network, Vadose Zone Journal, 12(3), 918-924,
461 2013.
462 Döll, P., Fiedler, K. and Zhang, J.: Global-scale analysis of river flow alterations due to water
463 withdrawals and reservoirs, Hydrol. Earth Syst. Sci. 13 2413–32, 2009.

https://doi.org/10.5194/esd-2019-26
Preprint. Discussion started: 3 June 2019

464 Douville, H., Ribes, A., Decharme, B., Alkama, R. and Sheffield, J. Anthropogenic influence on
465 multidecadal changes in reconstructed global evapotranspiration, Nature Clim. Change 3, 59–62,
466 2013.
467 Feng, H. H., and Liu, Y. B.: Trajectory based detection of forest-change impacts on surface soil moisture
468 at a basin scale [Poyang Lake Basin, China], J. Hydrol. 514, 337–346, 2014.
469 Feng, H. H., and Zhang, M. Y.: Global land moisture trends: drier in dry and wetter in wet over land,
470 Sci. Rep. 5, 18018; doi: 10.1038/srep18018, 2015.
471 Feng, H. H.: Individual contributions of climate and vegetation change to soil moisture trends across
472 multiple spatial scales, Sci. Rep. 6, 32782; doi: 10.1038/srep32782, 2016.
473 Guo, Z., Dirmeyer, P., Zeng, Z. H., Gao, X., and Zhao, M.: Evaluation of the Second Global Soil
474 Wetness Project soil moisture simulations: 2. Sensitivity to external meteorological forcing, J.
475 Geophys. Res., 111, D22S03, https://doi.org/10.1029/2006JD007845, 2006.
476 Haddeland, I., Clark, D. B., Franssen, W., Ludwig, F., Voß, F., Arnell, N. W., Bertrand, N., Best, M.,
477 Folwell, S., Gerten, D., Gomes, S., Gosling, S. N., Hagemann, S., Hanasaki, N., Harding, R.,
478 Heinke, J., Kabat, P., Koirala, S., Oki, T., Polcher, J., Stacke, T., Viterbo, P., Weedon, G. P., and
479 Yeh, P.: Multimodel Estimate of the Global Terrestrial Water Balance: Setup and First Results,
480 Journal of Hydrometeorology., 12, 869–884, 2011.
481 Hulme, M.: Rainfall changes in africa: 1931–1960 to 1961–1990, International Journal of Climatology,
482 12(7), 685-699, 1992.
483 Hurtt, G. C., Chini, L. P., Frolking, S., Betts, R. A., Feddema, J., Fischer, G., Fisk, J. P., Hibbard, K.,
484 Houghton, R. A., Janetos, A., Jones, C. D., Kindermann, G., Kinoshita, T., Goldewijk, K. K., Riahi,
485 K., Shevliakova, E., Smith, S., Stehfest, E., Thomson, A., Thornton, P., van Vuuren, D. P., and

https://doi.org/10.5194/esd-2019-26
Preprint. Discussion started: 3 June 2019

Wang, Y. P.: Harmonization of land-use scenarios for the period 1500–2100: 600 years of global gridded annual land-use transitions, wood harvest, and resulting secondary lands, Climatic Change, 109(1-2), 117, 2011.

Jia, B. H., Liu, J. G., Xie Z. H., and Shi, C. X.: Interannual variations and trends in remotely sensed and modeled soil moisture in China, Journal of Hydrometeorology. 19, 831-847, 2018.

Kim, H., Watanabe, S., Chang, E-.C., Yoshimura, K., Compo, G. P., Hirabayashi, Y., Famiglietti, J., and Oki, T.: A century-long global surface meteorology for offline terrestrial simulations, in preparation, 2016.

Kowalczyk, E.A., Wang, Y.P., Law, R.M., Davies, H.L., McGregor, J.L., and Abramowitz, G.: The CSIRO Atmosphere Biosphere Land Exchange (CABLE) model for use in climate models and as an offline model. CSIRO Marine and Atmospheric Research Paper 013: http://www.cmar.csiro.au/e-print/open/kowalczykea_2006a.pdf, 2006.

Kottek, M., Grieser, J., Beck, C., Rudolf, B. and Rubel, F.: World Map of the Köppen-Geiger climate classification updated, Meteorol. Z15, 259–263, 2006.

Lawrence, D. M., Oleson, K. W., Flanner, M. G., Thorton, P. E., Swenson, S. C., Lawrence, P. J., Zeng, X. B., Yand, Z. L., and Levis, S.: Parameterization improvements and functional and structural advances in version 4 of the Community Land Model, Journal of Advances in Modeling Earth Systems, 3, M03001, 2011.

L' Hôte Y, Mahé G, Somé B, and Triboulet JP.: Analysis of a sahelian annual rainfall index from 1896 to 2000; the drought continues, International Association of Scientific Hydrology Bulletin, 47(4), 10, 2002.

https://doi.org/10.5194/esd-2019-26
Preprint. Discussion started: 3 June 2019

507 Marczewski, W., Slominski, J., Slominska, E., Usowicz, B., Usowicz, J., Romanov, S., Maryskevych,
508 O., Nastula, J., and Zawadzki, J.: Strategies for validating and directions for employing SMOS
509 data, in the Cal-Val project SWEX (3275) for wetlands. Hydrology and Earth System Sciences
510 Discussions, 7, 7007–7057, 2010.
511 Min, S-K., Zhang, X. B., Zwiers, F. W. and Hegerl, G. C.: Human contribution to more-intense
512 precipitation extremes, Nature 470, 378–382, 2011.
513 Mougin, E., Hiernaux, P., Kergoat, L., Grippa, M., de Rosnay, P., Timouk, F., Le Dantec, V., Demarez,
514 V., Lavenu, F., Arjounin, M., Lebel, T., Soumaguel, N., Ceschia, E., Mougenot, B., Baup, F.,
515 Frappart, F., Frison, P. L., Gardelle, J., Gruhier, C., Jarlan, L., Mangiarotti, S., Sanou, B., Tracol,
516 Y., Guichard, F., Trichon, V., Diarra, L., Soumaré, A., Koité, M., Dembélé, F., Lloyd, C., Hanan,
517 N. P., Damesin, C., Delon, C., Serca, D., Galy-Lacaux, C., Seghieri, J., Becerra, S., Dia, H.,
518 Gangneron, F., and Mazzega, P.: The AMMA-CATCH Gourma observatory site in Mali: Relating
519 climatic variations to changes in vegetation, surface hydrology, fluxes and natural resources.
520 Journal of Hydrology, 375, 14–33, 2009.
521 Oleson, K: Technical description of version 4.5 of the Community Land Model (CLM), NCAR Tech.
522 Note NCAR/TN-503+ STR, Boulder, Colo., 420pp, 2013.
523 Pellarin, T., Laurent, J. P., Cappelaere, B., Decharme, B., Descroix, L., and Ramier, D.: Hydrological
524 modelling and associated microwave emission of a semi-arid region in South-western Niger.
525 Journal of Hydrology, 375, 262–272, 2009.
526 Robock, A., Vinnikov, K. Y., Srinivasan, G., Entin, J. K., Hollinger, S. E., Speranskaya, N. A., Liu, S.
527 X., and Namkhai, A.: The Global Soil Moisture Data Bank, Bull. Amer. Meteor. Soci., 81, 1281-
528 1299, 2000.

https://doi.org/10.5194/esd-2019-26
Preprint. Discussion started: 3 June 2019

529 Robock, A., Mu, M., Vinnikov, K., Trofimova, I. V., and Adamenko T. I.: Forty-five years of observed
530 soil moisture in the Ukraine: No summer desiccation (yet), Geophys. Res. Lett., 32, L03401,
531 doi:10.1029/2004GL021914, 2005.
532 Siebert, S., Döll, P., Hoogeveen, J. , Faures, J. M., Frenken, K., and Feick, S.: Development and
533 validation of the global map of irrigation areas, Hydrology and Earth System Sciences, 9, 535–547,
534 2005.
535 Sen, P. K.: Estimates of the regression coefficient based on Kendall's tau, J. Amer. Stat. Assoc., 63,
536 1379–1389, 1968.
537 Seneviratne, S., Corti, T., Davin, E., Hirschi, M., Jaeger, E., Lehner, I., Orlowsky, B., and Teuling, A.:
538 Investigating soil moisture–climate interactions in a changing climate: A review, Earth-Sci. Rev.,
539 99, 125–161, 2010.
540 Sheffield, J. , Goteti, G. , and Wood, E. F.: Development of a 50-year high-resolution global dataset of
541 meteorological forcings for land surface modeling, J. Climate, 19(13), 3088--3111, 2006.
542 Smith, A. B., Walker, J. P., Western, A. W., Young, R. I., Ellett, K. M., Pipunic, R. C., Grayson, R. B.,
543 Siriwardena, L., Chiew, F. H. B., and Richter, H.: The Murrumbidgee soil moisture monitoring
544 network dataset. Water Resources Research, 48(7), 7701, 2012.
545 Taylor, and Karl, E.: Summarizing multiple aspects of model performance in a single diagram, Journal
546 of Geophysical Research, 106(D7):7183, 2001.
547 Van Den Hurk, B., Best, M., Dirmeyer, P., Pitman, A., Polcher, J., and Santanello, J.: Acceleration of
548 Land Surface Model Development over a Decade of Glass, Bull. Amer. Meteor. Soci., 92, 1593–
549 1600. doi:10.1175/BAMS-D-11-00007.1, 2011.

https://doi.org/10.5194/esd-2019-26
Preprint. Discussion started: 3 June 2019

550 Van Den Hurk, B., Kim, H. J., Krinner, G., Seneviratne, S.I., Derksen, C., Oki, T., Douville, H., Colin,
551 J., Ducharne, A., Cheruy, F., Viovy, N., Puma, M.J., Wada, Y., Li, W., Jia, B. H., Alessandri, A.,
552 Lawrence, D.M., Weedon G.P., Ellis, R., Hagemann, S., Mao, J., Flanner, M.G., Zampieri, M.,
553 Materia, S., Law, R.M., Sheffield, J.: LS3MIP (V1.0) contribution to CMIP6: The Land Surface,
554 Snow and Soil moisture Model Intercomparison Project – aims, setup and expected outcome,
555 Geosci. Model Dev., 9, 2809–2832, 2016.
556 Viovy, N., and Ciais, P.: A combined dataset for ecosystem modelling:
557 http://esgf.extra.cea.fr/thredds/catalog/store/ p529viov/cruncep/catalog.html, last access: 1 August
558 2016, 2009.
559 Wada, Y., Van Beek, L. P. H., Wanders, N., and Bierkens, M. F. P.: Human water consumption
560 intensifies hydrological drought worldwide, Environmental Research Letters, 2013,
561 8(3):034036,2013.
562 Wagner, W., Lemoine, G., and Rott, H.: A method for estimating soil moisture from ERS scatterometer
563 and soil data, Remote Sens. Environ, 70(2), 191-207, 1999.
564 Wang, A. H., and Zeng, X. B.: Sensitivities of terrestrial water cycle simulations to the variations of
565 precipitation and air temperature in China, J. Geophys. Res: Atmospheres, 2011, 116(D2) , 2011.
566 Weedon, G. P., Balsamo, G., Bellouin, N., Gomes, S., Best, M. J., and Viterbo, P.: The WFDEI
567 meteorological forcing dataset: WATCH Forcing Data methodology applied to ERAInterim
568 reanalysis data, Water Resour. Res., 50, 7505–7514, 2014.
569 Wei, J., Dirmeyer, P. A., and Guo, Z.: Sensitivities of soil wetness simulation to uncertainties in
570 precipitation and radiation, Geophys. Res. Lett., 35, L15703. doi:10.1029/2008GL034494, 2008.

https://doi.org/10.5194/esd-2019-26
Preprint. Discussion started: 3 June 2019

571 Wentz, F. J., Ricciardulli, L., Hilburn, K. and Mears, C.: How Much More Rain Will Global Warming
572 Bring? Science 13, 233–235, 2007.
573 Wisser, D., Fekete, B. M., Vörösmarty, C. J. and Schumann, A. H.: Reconstructing 20th century global
574 hydrography: acontribution to the global terrestrial network-hydrology (GTNH), Hydrol. Earth
575 Syst. Sci., 14 1–24, 2010
576 Xie Z. H., Liu S., Zeng Y. Y., Gao J. Q., Qin P. H., Jia, B. H., Xie, J. B., Liu, B., Li, R. C., Wang, Y.,
577 and Wang, L. H.: A high-resolution land model with groundwater lateral flow, water use and soil
578 freeze-thaw front dynamics and its applications in an endorheic basin, J. Geophys. Res.-Atmos.,
579 123, 7204-7222. https://doi.org/10.1029/2018JD028369, 2018.
580 Yin, Z., Ottlé, C., Ciais, P., Guimberteau, M., Wang, X. H., Zhu, D., Maignan, F., Peng, S. S., Piao, S.
581 L., Polcher, J., Zhou, F., Kim, H., and other China-Trend-Stream project members.: Evaluation of
582 ORCHIDEE-MICT-simulated soil moisture over China and impacts of different atmospheric
583 forcing data, Hydrol. Earth Syst. Sci., 22, 5463–5484, https://doi.org/10.5194/hess-22-5463-2018,
584 2018.
585 Yu, Y., Xie, Z. H., and Zeng, X. B.: Impacts of modified Richards equation on RegCM4 regional climate
586 modeling over East Asia, J. Geophys. Res.-Atmos., 119, 12642–12659, doi:10.1002/2014jd021872,
587 2014.
588 Zeng, Y. Y., Xie, Z. H., and Liu, S.: Seasonal effects of irrigation on land-atmosphere latent heat,
589 sensible heat, and carbon fluxes in semiarid basin, Earth System Dynamics, 8(1), 113–127, 2017.
590 Zeng, Y. Y., Xie, Z. H., Yu, Y., Liu, S., Wang, L. Y., Zou, J., Qin, P. H., and Jia, B. H.: Effects of
591 anthropogenic water regulation and groundwater lateral flow on land processes, Journal of
592 Advances in Modeling Earth Systems, 8(3), 1106–1131, 2016a.

https://doi.org/10.5194/esd-2019-26
Preprint. Discussion started: 3 June 2019

593 Zeng, Y. Y., Xie, Z. H., and Zou, J.: Hydrologic and climatic responses to global anthropogenic
594 groundwater extraction, J. Climate, 30. 10.1175/JCLI-D-16-0209.1, 2016b.
595 Zhan, X., Zheng, W., Fang, L., Liu, J., Hain, C., Yin, J., and Ek, M.: A preliminary assessment of the
596 impact of SMAP soil moisture on numerical weather forecasts from GFS and NUWRF models,
597 IGARSS 2016 - 2016 IEEE International Geoscience and Remote Sensing Symposium, IEEE,
598 5229–5232, 2016.
599 Zou, J., Xie, Z. H., Yu, Y., Zhan, C. S., and Sun, Q.: Climatic responses to anthropogenic groundwater
600 exploitation: A case study of the Haihe River Basin, northern China, Climate Dyn., 42 , 2125–2145,
601 2014.

https://doi.org/10.5194/esd-2019-26
Preprint. Discussion started: 3 June 2019

Earth System Dynamics
Discussions
Open Access
EGU

602 Tables

603 **Table 1.** General information of the meteorological forcing datasets

Data	Spatial	Interval	Time period	Source
GSWP	0.5°	3-hourly	1901–2012	[Kim et al., 2016]
WFD/WFDEI	0.5°	3-hourly	1901–2000/1979–2014	[Haddeland et al., 2011; Weedon at al., 2014]
CRU-NCEP	0.5°	6-hourly	1901–2010	[Viovy and Ciais, 2009]
PRINCETON	0.5°	3-hourly	1901–2012	[Sheffield et al., 2006]

604

605

606 **Table 2.** Details for the stations used in this study.

Continent	Network name	Country	Number of sites used	Depths (m)	Corresponding simulated soil layer	References
Africa	AMMA-CATCH	Benin, Niger	4	0.05;0.2,0.4	3,5,6	Cappelaere et al. (2009); de Rosnay et al. (2009); Mougin et al. (2009); Pellarin et al. (2009)
Australia	OZNET	Australia	8	0–0.3;0.3–0.6; 0.6–0.9	1–5;6–7;7	Smith et al. (2012)
Europe	SMOSMANIA, ORACLE, SWEX_POLAND	France, Poland	20	0.05;0.1; 0.2;0.3	3;4;5;6	Albergel et al. (2008); Calvet et al. (2008); https://bdoh.irstea.fr/ORACLE/ Marczewski et al. (2010)
North America	SNOTEL, SCAN	US	82	0.05;0.2;0.5	3;5;6–7	http://www.wcc.nrcs.usda.gov/snow/ http://www.wcc.nrcs.usda.gov/scan/
Asia	IIT_KANPUR	India	1	0.1;0.25; 0.5;0.8	4;5;6–7;7	http://www.iitk.ac.in/
Asia	CHINA	China	40	0–0.1;0.1–0.2; 0.2–0.3;0.3–0.5	1–3;4;5;7	Robock et al. (2000)

https://doi.org/10.5194/esd-2019-26
Preprint. Discussion started: 3 June 2019

Earth System Dynamics
Discussions
Open Access
EGU

Asia	MONGOLIA	Mongolia	28	0–0.1,0.1–0.2, 0.2–0.3	1–3;4;5	Robock et al. (2000)
Asia	RUSWET-GRASS	Former Soviet Union	30	0–0.1,0–1	1–3;1–8	Robock et al.(2000)

https://doi.org/10.5194/esd-2019-26
Preprint. Discussion started: 3 June 2019

Earth System Dynamics
Discussions
Open Access
EGU

609 **Table 3.** Trends in NEW simulated surface soil moisture and precipitation and
610 temperature of forcing data. * = $p < 0.05$.

NEW	SM ($m^3m^{-3}yr^{-1}$)	Pre ($mmyr^{-1}$)	Tem ($°C\ yr^{-1}$)
GSWP	*−0.89e−4	−0.16	*0.017
CRU-NCEP	*−0.97e−4	−0.27	*0.017
PRINCETON	−0.65e−4	−0.008	*0.017
WFD	*−0.15e−3	*−1.96	*0.019

611

612

https://doi.org/10.5194/esd-2019-26
Preprint. Discussion started: 3 June 2019

Earth System Dynamics
Discussions
Open Access
EGU

613 **Figures**

614

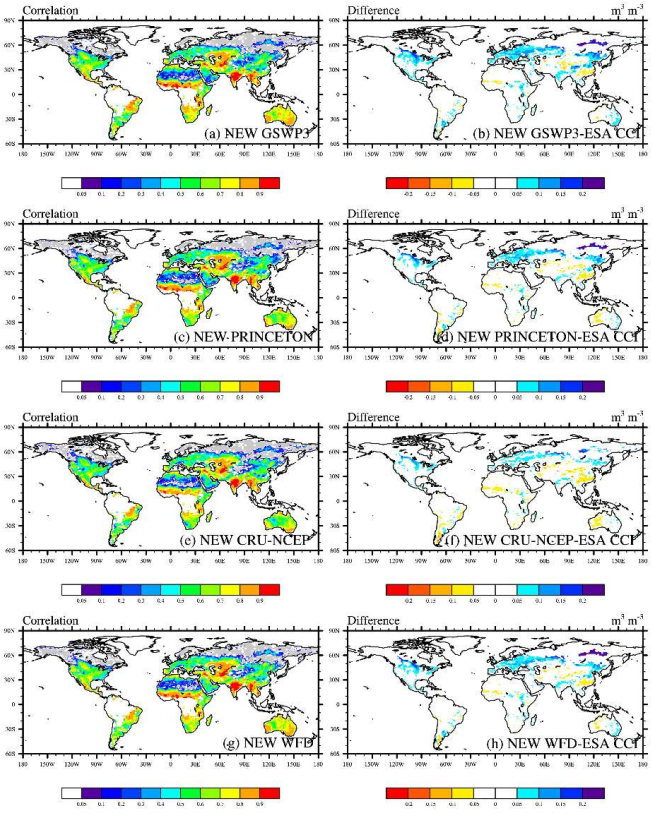

615

616 **Figure 1.** Correlation coefficients (a, c, e, g) and differences of spatial patterns (b, d, f, h) of the ESA CCI soil
617 moisture and the corresponding simulated top 10 cm soil moisture from 1979–2010. Gray pixels indicate no
618 correlation and negative correlation.

619

https://doi.org/10.5194/esd-2019-26
Preprint. Discussion started: 3 June 2019

Earth System Dynamics
Discussions
Open Access
EGU

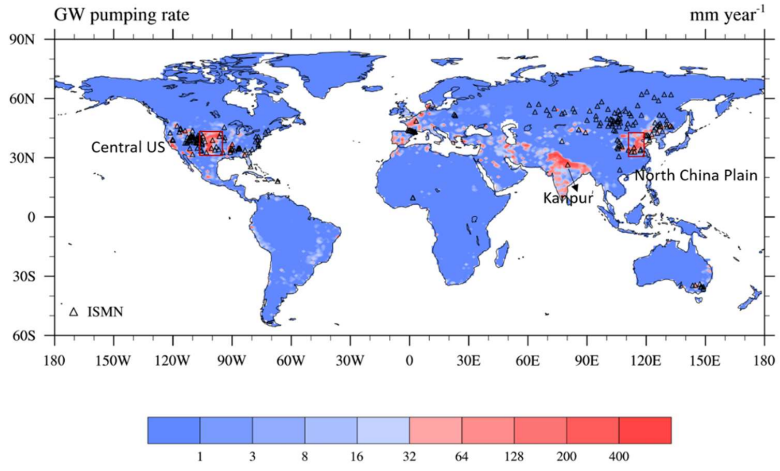

620

621 **Figure 2.** Distribution of soil moisture stations and three subregions. Seven stations on the North China Plain, 15
622 in central US, and one in Kanpur of North India). The background is the groundwater (GW) extraction rate.

623

https://doi.org/10.5194/esd-2019-26
Preprint. Discussion started: 3 June 2019

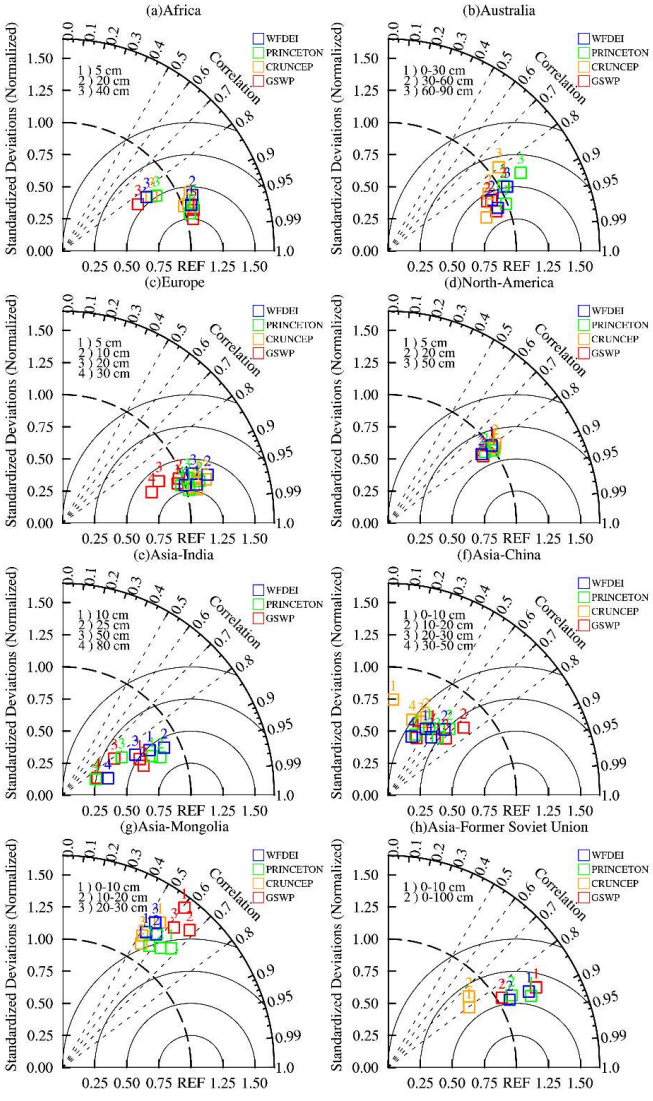

Figure 3. Taylor diagrams illustrating the comparisons among GSWP, CRUNCEP, PRINCETON, WFDEI, and in-situ observation data.

https://doi.org/10.5194/esd-2019-26
Preprint. Discussion started: 3 June 2019

Earth System Dynamics
Discussions
Open Access
EGU

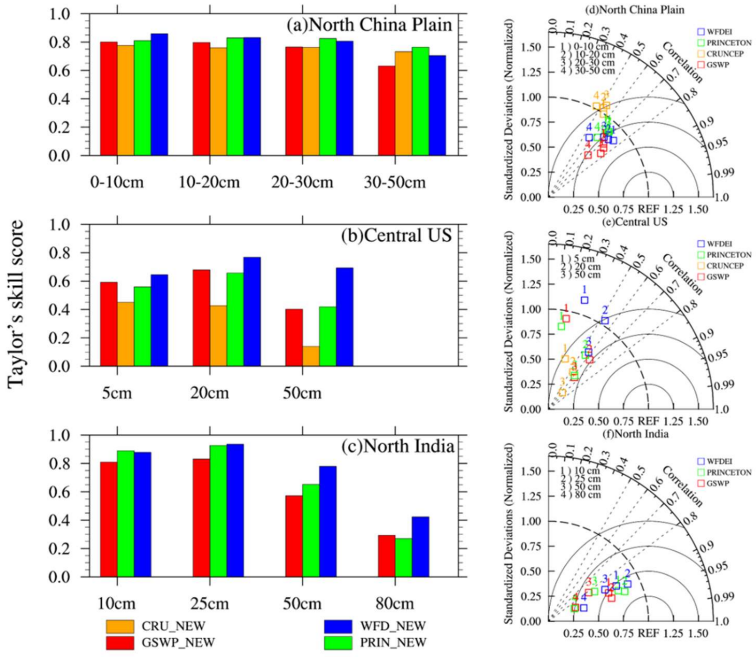

627

628 **Figure 4.** Taylor's skill scores and Taylor diagrams illustrating the comparisons among GSWP, CRUNCEP,
629 PRINCETON, WFDEI, and in-situ observations. (a, d) North China Plain; (b, e) Colorado of Central US; (c, f) North
630 India. The azimuthal angle represents the correlation coefficient, and radial distance is the standard deviation
631 normalized to observations.

https://doi.org/10.5194/esd-2019-26
Preprint. Discussion started: 3 June 2019

Earth System Dynamics
Discussions
Open Access
EGU

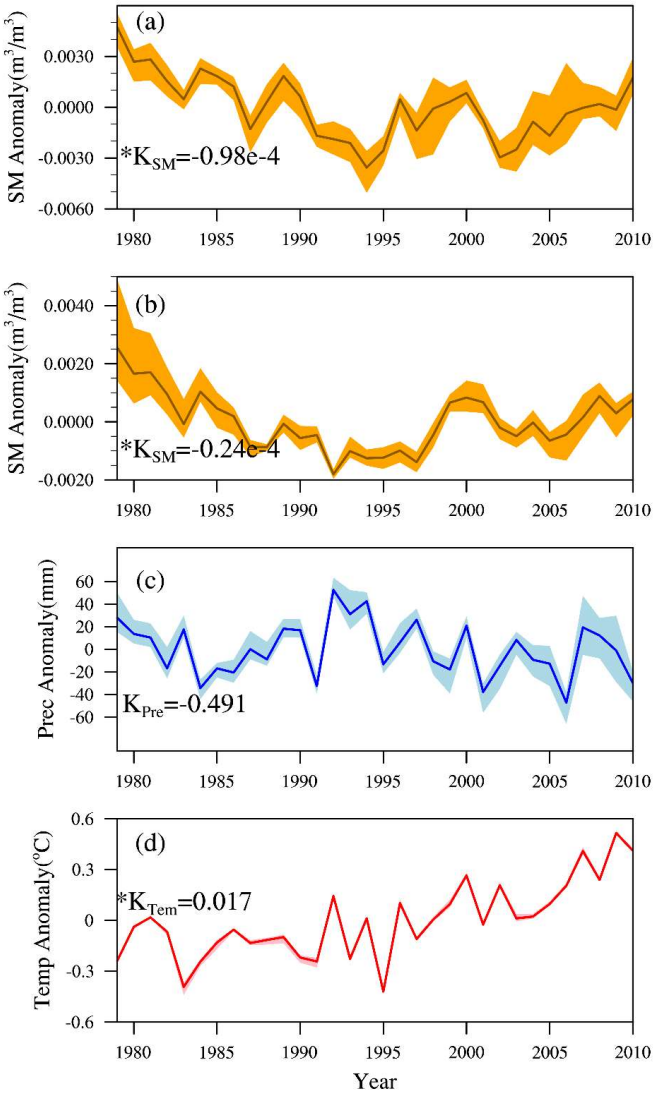

632

633 **Figure 5.** Annual mean of (a) surface soil moisture, (b) deep soil moisture, (c) precipitation, and (d) temperature
634 averaged globally from 1979–2010. * = $p < 0.05$.

635

https://doi.org/10.5194/esd-2019-26
Preprint. Discussion started: 3 June 2019

Earth System Dynamics
Discussions
Open Access
EGU

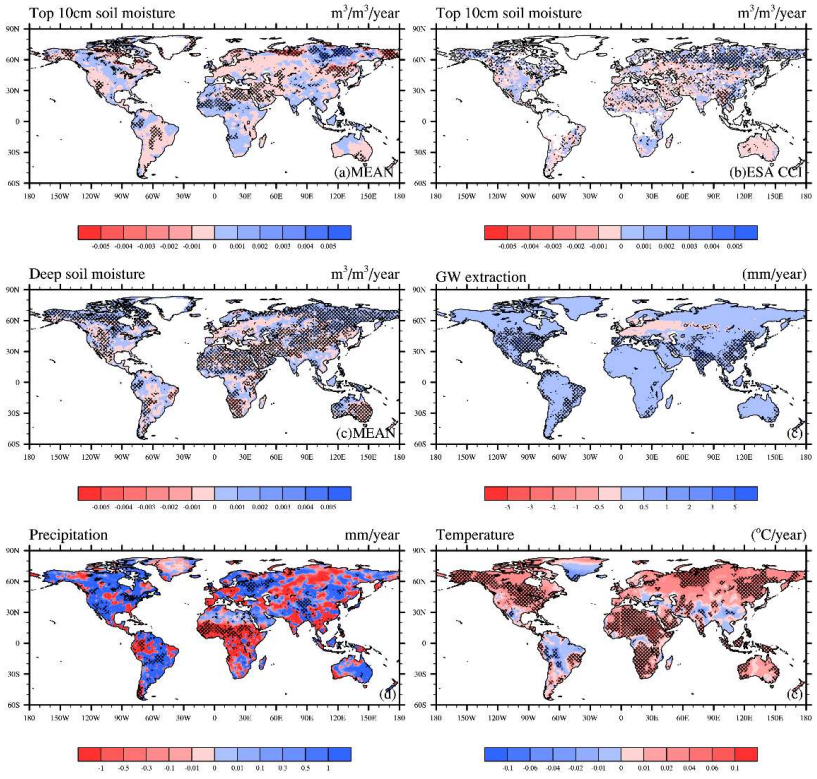

636

637 **Figure 6.** The spatial distribution of linear trends for (a) and (b) surface soil moisture (m^{-3} yr^{-1}), (c) deep soil
638 moisture (m^{-3} yr^{-1}) , (d) and (e) precipitation (mm yr^{-1}), temperature (°C yr^{-1}), groundwater extraction (mm yr^{-1}).
639 The shaded areas represent grids with statistically significant trends ($p < 0.05$).

640

https://doi.org/10.5194/esd-2019-26
Preprint. Discussion started: 3 June 2019

Earth System Dynamics
Discussions
Open Access
EGU

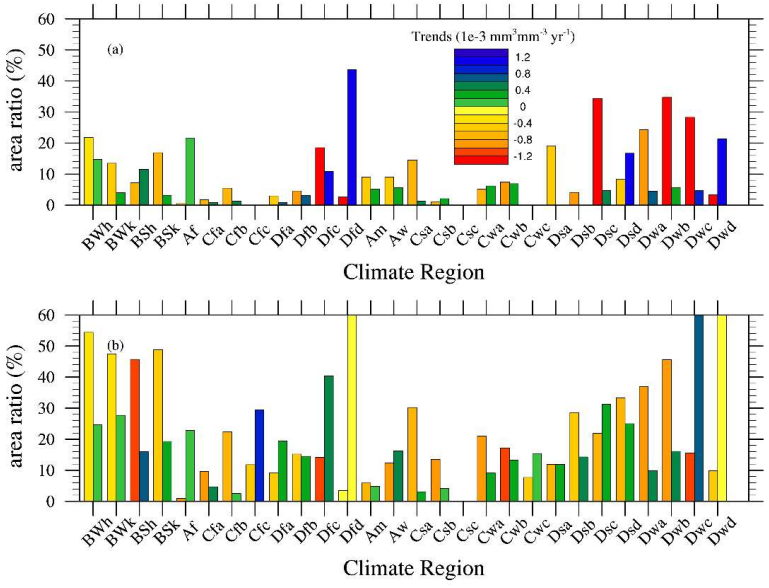

641

642 **Figure 7.** Statistics of the soil moisture trends. (a, b) The ratio of surface and deep soil moisture to wet and dry for
643 28 Köppen-Geiger climate types. For each type, the left bar is the drying ratio and the right bar is the wetting ratio.

644

https://doi.org/10.5194/esd-2019-26
Preprint. Discussion started: 3 June 2019

Earth System Dynamics
Discussions
Open Access
EGU

645

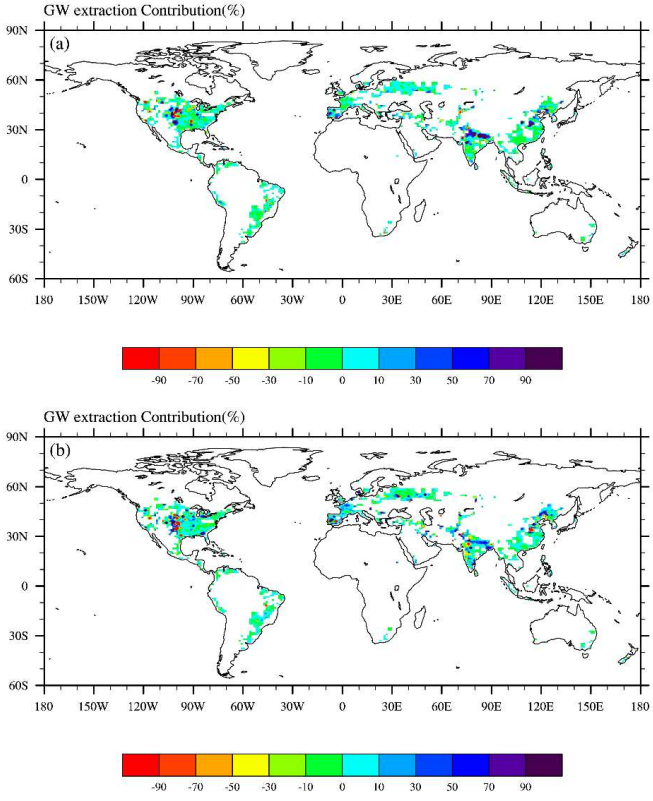

646

647

648 **Figure 8.** The relative contribution of groundwater extraction to (a) surface and (b) deep soil moisture trends (%).

649

https://doi.org/10.5194/esd-2019-26
Preprint. Discussion started: 3 June 2019

Earth System Dynamics
Discussions
Open Access
EGU

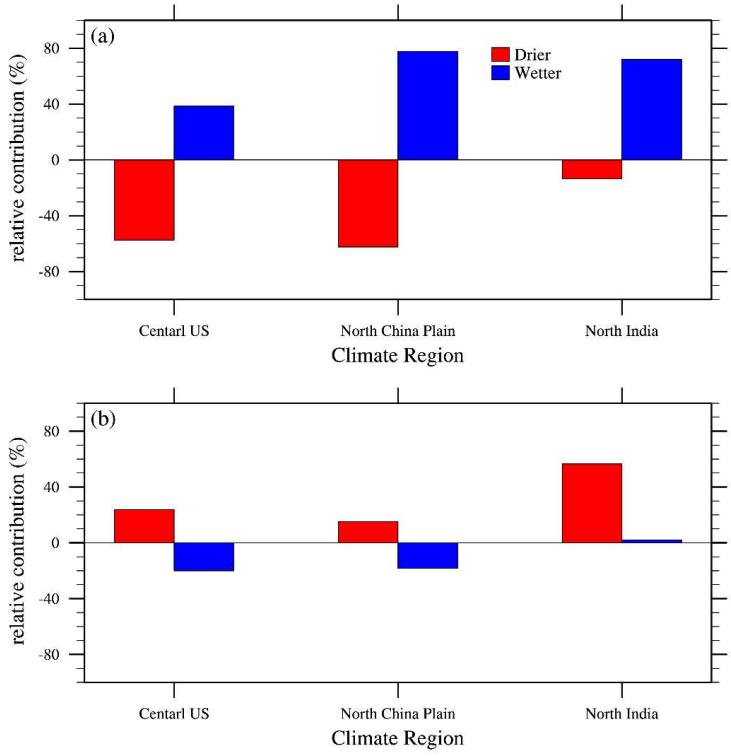

650

651 **Figure 9.** The relative contribution of GW extraction to regional (a) surface, (b) deep soil moisture trends (%). North
652 China Plain (34N–40N, 110E–120E), northern India (23N–33N, 68E–78E), central US (33N–42N, 97W–105W).